# Research Update: Bismuth based materials for photovoltaics

Nichole Cates Miller[1] and María Bernechea[2,3,a]

[1]*Smart Material Solutions, Inc., Raleigh, North Carolina 27607, USA*
[2]*ARAID, Government of Aragon, 50018 Zaragoza, Spain*
[3]*Institute of Nanoscience of Aragon (INA), University of Zaragoza, 50018 Zaragoza, Spain*

In this Research Update, we briefly summarize some of the bismuth materials that have been investigated for their use in photovoltaic solar cells. We focus on bismuth-based perovskites and bismuth halides, as alternatives to lead-halide perovskites, and bismuth-based sulfides ($Bi_2S_3$, $Cu_xBi_yS_z$, and $AgBiS_2$), as alternatives to lead sulfide quantum dots. These materials fulfill the requirements of being composed of abundant and non-toxic elements. Moreover, they exhibit adequate properties for photovoltaics like high absorption coefficients and suitable bandgaps, plus additional attractive characteristics in terms of robustness and stability. However, they have not been extensively studied and therefore their efficiencies are still far from those reported for their toxic counterparts. Here we collect some of the most promising results, point at possible limiting factors, and suggest some routes to improve performance. © *2018 Author(s). All article content, except where otherwise noted, is licensed under a Creative Commons Attribution (CC BY) license (http://creativecommons.org/licenses/by/4.0/).* https://doi.org/10.1063/1.5026541

## I. INTRODUCTION

Perovskites and inorganic quantum dot solar cells offer the highest efficiencies among the "emerging PV" technologies.[1] They also have the potential to be flexible and less expensive, thinner, and efficient over a wider range of light intensities than traditional or other emerging technologies. Furthermore, they can be composed of abundant elements, which is important both for reducing costs and assuring future production.[2,3]

However, the best performing devices have been fabricated using materials that have lead (Pb) in their composition: PbS or $CsPbI_3$ in quantum dot solar cells[4,5] or $APbI_3$ (A = methylammonium or formamidinium) in perovskite solar cells.[6] Although the concept and extent of toxicity can be discussed, the fact is that lead is listed among the 10 chemicals of major public health concern by the World Health Organization[7] and its use is restricted under several legislations worldwide, therefore compromising the future commercialization of solar cells based on these materials.[8]

In this sense, bismuth-based materials can be interesting alternatives for replacing lead-containing compounds. Bismuth is a quite abundant metal on the earth crust; moreover, it is a by-product of Pb, Cu, and Sn refining and has few significant commercial applications, resulting in the price of Bi being relatively low and stable (Fig. 1).[2,3,9] Additionally, despite being a heavy metal, bismuth is considered non-toxic and is even used in common medicines such as Pepto-Bismol.[10] Furthermore, $Bi^{3+}$ has been suggested as an excellent candidate for defect tolerant compounds, i.e., materials with good optoelectronic properties despite the presence of defects. Supposedly, the active $ns^2$ lone pair tends to create antibonding interactions at the valence band maximum, and as a result, defects are confined to shallow states at the band edges.[11,12]

In this Research Update, we will briefly summarize some of the bismuth materials that have been investigated for their use in photovoltaic solar cells. We will focus on bismuth-based perovskites

---

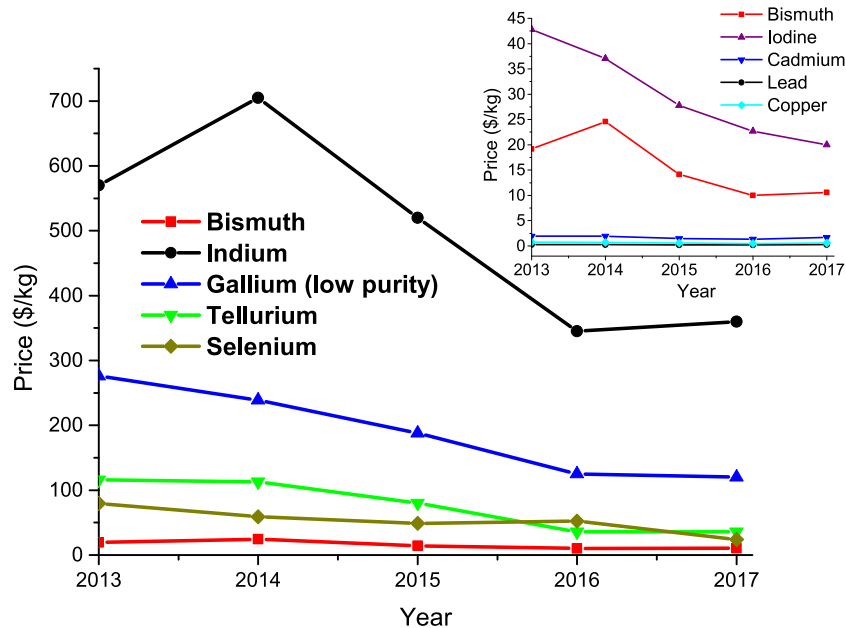[a]Author to whom correspondence should be addressed: mbernechea@unizar.es

FIG. 1. Price evolution of bismuth compared to other elements relevant for photovoltaics. Main figure: comparison with indium, gallium, tellurium, or selenium. Inset: comparison with iodine, cadmium, lead, and copper. Data extracted from the 2018 Mineral Commodity Summaries (https://minerals.usgs.gov/minerals/pubs/mcs/).

and bismuth halides, as alternatives to lead-halide perovskites, and bismuth-based sulfides ($Bi_2S_3$, $Cu_xBi_yS_z$, and $AgBiS_2$), as alternatives to lead sulfide quantum dots.

## II. BISMUTH-BASED PEROVSKITES AND BISMUTH HALIDES

Lead-based perovskite solar cells have attracted a huge amount of attention due to their rapid rise in efficiency, with $CH_3NH_3PbI_3$ solar cells recently achieving certified efficiencies in excess of 22%.[6] These materials can be solution processed and have a variety of promising characteristics including high absorption coefficients, large charge-carrier diffusion lengths, and relatively low exciton-binding energies,[13,14] closer to the binding energies reported for inorganic materials (6–15 meV), than those reported for organic solar cells (0.5 eV or larger).[15]

Still, commercialization of lead perovskite solar cells is hindered by their short lifetimes and the use of toxic lead.[16] Some hope that these limitations can be overcome by replacing lead with other elements like tin,[17] antimony,[18] or bismuth.[11,16,19] Bismuth-based analogs to lead perovskite photovoltaic materials offer great promise for future development, although they have been scarcely explored.

Bismuth perovskites generally have the chemical formula $A_3Bi_2X_9$, where A is a monovalent cation (i.e., $Cs^+$ or $CH_3NH_3^+$) and X is a halogen anion (i.e., $Cl^-$, $Br^-$, and/or $I^-$). $(CH_3NH_3)_3Bi_2I_9$ and $Cs_3Bi_2I_9$ are two bismuth perovskite materials that have been investigated thanks to their similarities to their high-efficiency lead counterparts $CH_3NH_3PbI_3$ and $CsPbI_3$, respectively.

The crystal structure of $Cs_3Bi_2I_9$ was initially studied in the 1960s.[20] Almost 50 years later, Park *et al.* first incorporated bismuth perovskite materials into solar cells, demonstrating power-conversion efficiencies of 1.09% for $Cs_3Bi_2I_9$ and 0.12% for $(CH_3NH_3)_3Bi_2I_9$.[21] These modest efficiencies were attributed to high exciton binding energies (70-300 meV compared to 8-20 meV for lead perovskites[22–24]), significant non-radiative recombination due to defect states,[25] non-optimal charge-extraction layers, and high bandgaps (2.1-2.2 eV). Despite their modest efficiencies, these materials exhibited high absorption coefficients and were much more air-stable than their lead counterparts.

The good stability of bismuth perovskites in both dry and humid air has since been repeatedly demonstrated. For instance, $(CH_3NH_3)_3Bi_2I_9$ exhibited stable photovoltaic performance during
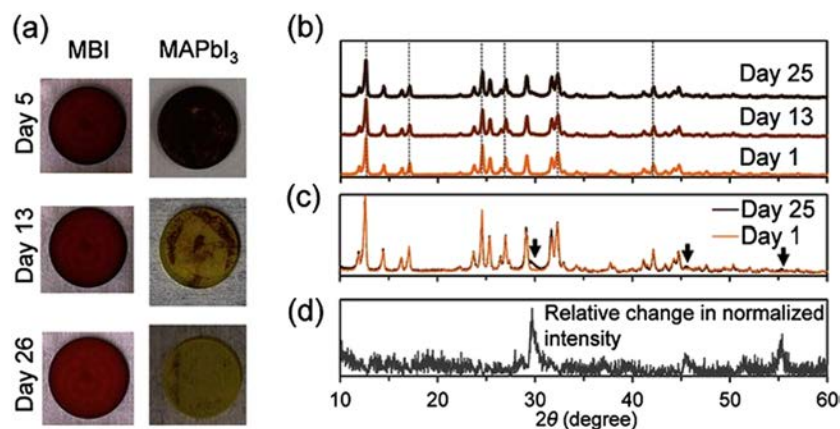
FIG. 2. (a) Photographs of methylammonium bismuth iodide (MBI) and methylammonium lead iodide (MAPbI$_3$) over-time in ambient air. [(b) and (c)] Normalized XRD patterns of MBI over time with air exposure. (d) The relative change in the normalized intensity of the diffraction peaks of MBI (day 25 vs. day 1). Reproduced with permission from Hoye *et al.*, "Methylammonium bismuth iodide as a lead-free, stable hybrid organic-inorganic solar absorber," Chem. - Eur. J. **22**, 2605–2610 (2016). Copyright 2016 Wiley-VCH Verlag GmbH and Co. KGaA.

10 weeks in ambient air[26] and 21 days in air with an average humidity of ~50%.[27] In another study, x-ray diffraction of (CH$_3$NH$_3$)$_3$Bi$_2$I$_9$ after 25 days in ambient air demonstrated almost no change other than the formation of a thin, protective oxidation layer that likely prevents further degradation (Fig. 2).[28] This is in stark contrast to the lead analog, CH$_3$NH$_3$PbI$_3$, which almost fully converted to PbI$_2$ during the same time period. Likewise, the bismuth perovskite exhibited only minimal visual changes after 26 days, whereas the lead analog changed from dark brown to light yellow after 5 days.

Further investigation of these and other bismuth perovskites has led to improvements in the material properties. In particular, many studies have attempted to tune the bandgaps of bismuth perovskites since unaltered bismuth perovskites tend to have bandgaps above 2 eV, which is higher than desirable for optimal solar-cell performance. For example, one study demonstrated the ability to tune the bandgap of Cs$_2$AgBiBr$_6$ through pressure-induced changes in its crystal structure.[29] Others have shown that sulfur doping can decrease the bandgap of Cs$_3$Bi$_2$I$_9$ to a much more desirable value of 1.45 eV.[30,31]

Several groups have also improved the film quality and consequently the solar-cell performance of (CH$_3$NH$_3$)$_3$Bi$_2$I$_9$ by replacing standard solution-processing methods with alternative deposition methods that result in smoother, more compact films with fewer pinholes. For instance, Ran *et al.* used a two-step method that combines evaporation and spin coating to push the power conversion efficiency of (CH$_3$NH$_3$)$_3$Bi$_2$I$_9$ solar cells to 0.39%.[32] Zhang *et al.* later employed a two-step vacuum deposition method to fabricate (CH$_3$NH$_3$)$_3$Bi$_2$I$_9$ solar cells with a power conversion efficiency of 1.64% (0.83 V open-circuit voltage, 3.0 mA/cm$^2$ short-circuit current, and 0.79 fill factor).[33] The vacuum-processed solar cells exhibited charge-carrier diffusion lengths, trap densities, and absorption coefficients on par with many lead perovskite materials.

Likewise, new deposition techniques have resulted in improved Cs$_2$AgBiBr$_6$ film quality and consequently higher efficiencies. Cs$_2$AgBiBr$_6$ and its precursors exhibit low solubility in most common solvents, resulting in porous films full of cracks and pinholes. Dimethylsulfoxide (DMSO), on the other hand, has proven to be a good solvent for Cs$_2$AgBiBr$_6$ and its precursors: AgBr, CsBr, and BiBr$_3$. Gruel *et al.* therefore dissolved the precursors in DMSO, heated the solution, and spin coated it onto a heated substrate.[34] A subsequent annealing step at 250 °C was required to complete the formation of Cs$_2$AgBiBr$_6$ and maximize solar-cell performance. The best devices exhibited power-conversion efficiencies approaching 2.5% and an open-circuit voltage of 1.06 V, the highest value reported thus far for a bismuth-based perovskite. In a subsequent experiment, Gao *et al.* demonstrated the ability to deposit smooth films by dissolving Cs$_2$AgBiBr$_6$ in DMSO and spin coating the solution

using the anti-solvent dropping method with isopropanol (IPA) as the anti-solvent.[35] Films deposited without the anti-solvent were rough and frosted in appearance, whereas $Cs_2AgBiBr_6$ films deposited using the anti-solvent dropping method were very smooth and achieved efficiencies up to 2.2% and open-circuit voltages in excess of one volt. Again, a post-annealing treatment at 250 °C was required to produce high-quality, crystalline films.

Several related bismuth halides have also been explored as promising photovoltaic materials. For example, Kim *et al.* created dense, pinhole-free $AgBi_2I_7$ films by spin coating silver and bismuth precursors and subsequent annealing. The resulting air-stable material exhibited a bandgap of 1.87 eV and solar-cell efficiencies up to 1.22%.[36] Bismuth triiodide ($BiI_3$) has also been shown to be air-stable, to have a bandgap of ~1.8 eV, and to exhibit efficiencies up to 1.0%.[37–39]

One important distinction between bismuth perovskite and halide absorbers and their lead counterparts is the dimensionality of their octahedral networks. Figure 3 shows illustrations of 0D, 1D, 2D, and 3D octahedral networks and a few examples of bismuth perovskites and halides with each type of network. The octahedral network dimensionality can affect solar-cell performance by altering relevant material properties. Although there are notable exceptions, lower dimensional perovskites are usually associated with larger bandgaps, higher exciton binding energies, lower carrier mobilities, and better moisture stability due to more spatial confinement.[40–45]

The $CH_3NH_3PbI_3$ perovskite structure contains a 3D network of $PbI_6$ octahedra that share corners in all three octahedral directions.[46] $Bi^{3+}$ cannot directly replace $Pb^{2+}$ in this 3D-perovskite structure due to its higher charge.[47] Charge neutrality forces the bismuth counterpart ($CH_3NH_3)_3Bi_2I_9$ into a 0D structure with face-sharing octahedra of $(Bi_2I_9)_3$ dimers that are separated by $(CH_3NH_3)^+$ ions.[48] The lack of a network between the $(Bi_2I_9)_3$ dimers has been blamed for lower carrier mobilities and a larger bandgap of $(CH_3NH_3)_3Bi_2I_9$ and $Cs_3Bi_2I_9$.[42] Double perovskites, which contain two different cations, offer one route to forming higher dimensional bismuth perovskites.[34,49] For example, $Cs_2AgBiBr_6$ has a 3D octahedral network and has demonstrated power-conversion efficiencies up to 2.43% as discussed previously.
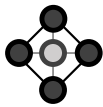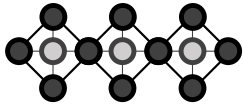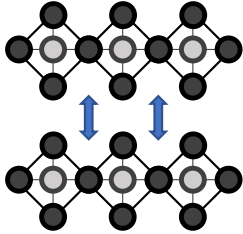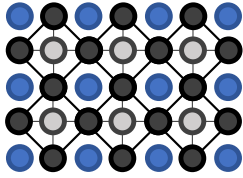
| Network Dimensionality | Structure Illustration | Examples (Efficiency) |
|---|---|---|
| 0D (No network) | | $Cs_3Bi_2I_9$ (1.09%)[21] $(CH_3NH_3)_3Bi_2I_9$ (1.64%)[33] $[HC-(NH_2)_2]_3Bi_2I_9$ (not reported)[40] |
| 1D (Network over one axis) | | $C_5H_6NBiI_4$ (0.9 %)[41] |
| 2D (Network over two axes) | | $K_3Bi_2I_9$ (not reported)[42] $Cs_3Bi_2Br_9$ (not reported)[43] |
| 3D (Network over three axes) | | $Cs_2AgBiBr_6$ (2.43%)[34] $AgBi_2I_7$ (1.22%)[36] |

FIG. 3. Illustrations and examples of some bismuth perovskite and halide absorbers with 0D, 1D, 2D, and 3D octahedral networks.

Although the efficiencies of bismuth perovskites and halides are currently modest, their demonstrated stability in humid air and their avoidance of toxic lead encourage further investigation. As many of these materials have yet to be extensively investigated, there remains considerable hope that the efficiencies can be significantly improved.

## III. BISMUTH SULFIDE (Bi₂S₃)

$Bi_2S_3$ is an n-type semicondcutor,[50] with a high absorption coefficient (in the range of $10^5$ cm$^{-1}$), and an absorption onset in the infrared. The reported bandgaps lie in the adequate region for photovoltaics and vary from 1.3 eV, for example in the bulk, to 1.7 eV, thanks to quantum confinement effects and/or stoichiometry variations.[51,52]

The first reports demonstrating the use of colloidal $Bi_2S_3$ nanocrystals (NCs) as an absorbing material in bilayer heterojunction solar cells employed as a p-type material either PbS quantum dots that had been exposed to ambient conditions (QDs)[53] or a conductive organic polymer like poly(3-hexylthiophene) (P3HT).[54] Both studies succeeded at demonstrating the $Bi_2S_3$ contribution to photocurrent by fabricating solar cells with ultra-small PbS QDs, with an absorption onset at 800 nm, or P3HT, with an absorption onset at 700 nm. The maximum efficiency obtained, 1.61% with PbS and 0.46% with P3HT, was modest but promising for a new material. Moreover, these studies already pointed to some factors limiting efficiency like high doping of the $Bi_2S_3$ films, poor electron mobility, and high recombination, most likely due to surface electron traps.

Efficiency was improved close to 5% by blending $Bi_2S_3$ NCs and PbS QDs to form a bulk nano-heterojunction structure.[55] The intimate mixing of the n- and p-type nanocrystalline semiconductors favors carrier transfer between materials, separating them more efficiently and reducing recombination. All these result in a prolonged lifetime and a threefold improvement in the short-circuit current. Similarly, when $Bi_2S_3$ NCs were blended with P3HT, or thiol-functionalized P3HT, an improvement in the short-circuit current provided an efficiency up to 1%.[56,57] Exploiting this same idea, performance was further improved when P3HT was blended with $Bi_2S_3$/Au Schottky diodes to fabricate hybrid bulk-heterojunction solar cells. The semiconductor-metal nanostructure augmented separation of charge carriers upon photogeneration and yielded an efficiency of 2%.[58]

Modifications in the solar cell structure is not the only strategy possible to improve efficiency. Changes in the synthesis enabled the production of $Bi_2S_3$ nanocrystals with different shapes and sizes, from $14 \times 19$ nm nanorods to spherical particles with a diameter of 2.6 nm; their performance in P3HT–$Bi_2S_3$ bilayer solar cells was studied.[52] The efficiency of the devices fabricated with the smaller nanocrystals was similar to analogous bilayer structures (0.43%),[54] but they showed an improved open-circuit voltage ($V_{oc}$), indicating reduced recombination, most likely due to a better surface passivation and a reduction of traps.

The ns$^2$ lone pair of $Bi^{3+}$ tends to be stereochemically active and produce highly anisotropic crystalline structures.[59,60] Indeed, $Bi_2S_3$ crystallizes in the orthorhombic system where tightly connected chains create layers that are connected through weak van der Waals forces that stack to form the final structure. This asymmetric structure produces preferential directions for electronic transport, enhanced along the c axis.[61]

In the examples mentioned above, nanocrystals are randomly oriented in the films (Fig. 4). Therefore, some of the NCs will be properly placed for conducting charges, while others will not, limiting charge transport and device efficiency. Considering this, strategies to create aligned $Bi_2S_3$ 1D structures like nanowires (NWs) or nanoribbons have been developed.[62,63] $Bi_2S_3$ NWs were vertically grown on a $TiO_2$-coated substrate, and spiro-OMeTAD was used as a hole transport layer. This structure suffered from high interfacial charge recombination, so a $Bi_2S_3$/$Ag_2S$ core-shell structure was developed and an efficiency of 2.5% was achieved.[62] In a different approach, $Bi_2S_3$ NWs were engineered to form percolated networks, where the interconnected nanowires provide a continuous path for electron transport. These porous networks were infiltrated with P3HT, forming a bulk-heterojunction and achieving a maximum efficiency of 3.3%.[63]
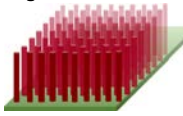
| Material (crystalline structure) | Nanomaterial aspect | Solar cell structure | Examples (Efficiency) |
|---|---|---|---|
| $Bi_2S_3$ (orthorhombic) | Randomly oriented rods/nanowires  | Bilayer heterojunction | $Bi_2S_3$-PbS (1.61 %)[53] <br> $Bi_2S_3$-P3HT (0.46 − 0.6 %)[52,54] |
| | | Bulk heterojunction | $Bi_2S_3$-PbS (5 %)[55] <br> $Bi_2S_3$-P3HT (1 %)[56,57] <br> $Bi_2S_3$/Au-P3HT (2 %)[58] |
| | Interconnected or aligned nanowires  | Nanostructured bilayer or "Bulk heterojunction" (infiltration in a network) | $Bi_2S_3$/$Ag_2S$-spiro-OMeTAD (2.5 %)[62] <br> $Bi_2S_3$-P3HT (3.3 %)[63] |
| $CuBiS_2$ (orthorhombic) | Nanoparticles  | Dye in DSSCs | $TiO_2$/$CuBiS_2$-$S_n^{2-}$/$nS^{2-}$ (0.62 %)[71] |
| | | Bilayer heterojunction | $TiO_2$-$CuBiS_2$-P3HT (0.68%)[72] |
| $Cu_3BiS_3$ (orthorhombic) | Nanosheets  | Dye in DSSCs | $TiO_2$ nanorod array/$Cu_3BiS_3$-$I^-$/$I^3$ (1.281 %)[77] |
| | Large area thin film  | Bilayer heterojunction | $Cu_3BiS_3$-CdS-ZnO (0.17 %)[78] |
| $Cu_4Bi_4S_9$ (orthorhombic) | Nanoribbons  | Bilayer heterojunction | ZnO nanowires-$In_2O_3$-$Cu_4Bi_4S_9$ (6.4 %)[80] <br> $\alpha$-$Fe_2O_3$-$Cu_4Bi_4S_9$/r-GO (7 %)[81] |
| $AgBiS_2$ (Cubic) | Nanoparticles  | Dye in DSSCs | $TiO_2$ nanorod array/$AgBiS_2$-$I^-$/$I^{3-}$ (0.95 %)[86] |
| | | Bilayer heterojunction | ZnO-$AgBiS_2$-PTB7 (6.3 %)[88] <br> ZnO-$AgBiS_2$-P3HT (4.3 %)[89] <br> ZnO-$AgBiS_2$-spiro-OMeTAD (1.5 %)[90] |

FIG. 4. Illustrations and examples of some bismuth-based sulfides used in different solar cell structures.

## IV. COPPER BISMUTH SULFIDES ($CuBiS_2$, $Cu_3BiS_3$, AND $Cu_4Bi_4S_9$)

Despite their potential application in many different areas, not only photovoltaics, the group of copper-bismuth sulfides has been scarcely explored. This is quite surprising, considering that all the elements are abundant and non-toxic and that analogous materials like $CuInS_2$, the copper-antimony family, and the copper-tin family have been the focus of several studies.[64–66]

Ternary Cu–Bi sulfides can show different stoichiometries and different properties. The three most studied compounds—$CuBiS_2$, $Cu_3BiS_3$, and $Cu_4Bi_4S_9$—crystallize in an orthorhombic structure and exhibit high absorption coefficients ($10^4$–$10^5$ cm$^{-1}$) and p-type character. These materials differ in their absorption onsets, and the reported bandgaps lie between 1.5 and 2.62 eV for $CuBiS_2$, 1.2 and 1.84 eV for $Cu_3BiS_3$, and 0.88–1.14 eV for $Cu_4Bi_4S_9$.[64,67]

### A. $CuBiS_2$

$CuBiS_2$ (emplectite) has been mostly studied from the theoretical point of view;[68–70] there are very few reports demonstrating the use of this material in photovoltaic solar cells (Fig. 4). In one experimental study, $CuBiS_2$ nanoparticles were deposited on $TiO_2$ using a chemical bath deposition method and used as sensitizers in dye sensitized solar cells (DSSCs) with a maximum efficiency of

0.62%.[71] More recently, $CuBiS_2$ was used a p-type material in planar heterojunction solar cells, sandwiched between $TiO_2$ and P3HT acting as hole and electron blocking layers, respectively. A maximum efficiency of 0.68% was achieved after doping the $CuBiS_2$ active layer with indium chloride.[72]

According to theoretical calculations, $CuBiS_2$ presents an indirect bandgap at 1.4–1.7 eV, however, the difference between indirect and direct bandgap energies is only 0.1–0.3 eV due to the rather flat lowest conduction band (CB); therefore, the direct transition is still accessible, and indeed the material exhibits high absorption coefficients (0.93–1.5 × $10^5$ cm$^{-1}$).[70,73] Interestingly, the $CuBiS_2$ density of states indicates that the formation of hole carriers will involve oxidation of Cu(I)–Cu(II). This may have implications for hole transport in $CuBiS_2$ and suggests that some Cu deficiencies may be beneficial, like in analogous photovoltaic materials such as CZTS.[69]

## B. $Cu_3BiS_3$

$Cu_3BiS_3$ (wittichenite) is of interest because it contains abundant non-toxic elements and presents p-type conductivity, a high absorption coefficient ($1 \times 10^5$ cm$^{-1}$), and reported experimental bandgaps between 1.2 and 1.84 eV.[64,74] Again, theoretical studies have calculated that the material exhibits a fundamental indirect bandgap at 1.5–1.7 eV, but the direct gap is close in energy (1.6–1.8 eV), showing promise as a solar absorber.[75] $Cu_3BiS_3$ nanocrystals were synthesized, and the corresponding nanocrystal-film showed a clear photoresponse in I–V measurements;[76] however, there are few studies reporting its incorporation in photovoltaic devices.

The first report on the efficiency of $Cu_3BiS_3$ employed nanosheets, obtained by a solvothermal route, that were used as a sensitizer on $TiO_2$ nanorods. The reported energy conversion efficiency of the $Cu_3BiS_3/TiO_2$ thin-film solar cell was a promising 1.281%.[77]

More recently, a $Cu_3BiS_3$ thin film was deposited by a dimethyl sulfoxide (DMSO)-based solution coating process and subsequent annealing in a nitrogen atmosphere. A solar cell combining wittichenite as a p-type material and CdS as an n-type semiconductor was fabricated, achieving a power conversion efficiency of 0.17%.[78] The authors attribute the quite low short-circuit current to an inadequate band alignment between the two semiconductors, indicating that improved efficiencies could be expected with a more appropriate n-type material.

## C. $Cu_4Bi_4S_9$

To date the highest efficiencies using copper-bismuth sulfides have been obtained employing $Cu_4Bi_4S_9$ (Fig. 4). As commented in Sec. III, the anisotropic orthorhombic structure can be responsible for the limited efficiency. Indeed, most of the studies on $Cu_4Bi_4S_9$ focus on the preparation of 1D structures (nanoribbons or nanobelts) and their incorporation in solar cells.

High conversion efficiencies, over 6%, have been observed for $Cu_4Bi_4S_9$ when nanoribbons obtained through a solvothermal method were used as p-type materials combined with n-type oxides, like $In_2O_3$ or $TiO_2$, and using $In_2S_3$ as a buffer layer.[79] Later the efficiency was increased to 6.4% by using n-type ZnO nanowires coated with an $In_2O_3$ buffer layer and $Cu_4Bi_4S_9$ as the absorber and hole transport layer.[80] More recently, efficiencies have approached 7% for bulk heterojunctions of $Cu_4Bi_4S_9$ and graphene oxide deposited on a $\alpha$-$Fe_2O_3$ layer.[81]

## V. $AgBiS_2$

In contrast to $Bi_2S_3$ and the copper-bismuth sulfide family, $AgBiS_2$ crystallizes in symmetrical crystalline structures: hexagonal at low temperatures, and a pseudo-cubic rock salt structure at high temperatures and as nanocrystals (Fig. 4). This fact enables possible omnidirectional transport of carriers.[82] Initial reports described $AgBiS_2$ as an n-type material with a favorable direct bandgap between 1.0 and 1.4 eV.[83,84]

As a first approach, $AgBiS_2$ nanocrystals were used as a sensitizer or counter-electrode in dye sensitized solar cells (DSSCs). The first $AgBiS_2$ nanoparticles were synthesized on $TiO_2$ using a sequential ionic layer adsorption reaction (SILAR) process. The liquid-junction semiconductor-sensitized solar cells fabricated with the photoanode showed a power conversion efficiency of 0.53% under 1 sun, and of 0.76% at a reduced light intensity of 0.148 sun.[85] More recently, a $TiO_2$ nanorod

array was decorated with $AgBiS_2$ nanocrystals electrochemically deposited, reaching a maximum efficiency of 0.95%.[86] Using a related approach, $AgBiS_2$ nanocrystals were synthesized by a solvothermal process and used as a contra-electrode in a polysulfide electrolyte DSSC. The overall power conversion efficiency was 2.09%, higher than the reference device using platinum as a counter-electrode (1.73%).[87]

Finally, $AgBiS_2$ nanocrystals were used as an active layer in solution-processed solar cells. The effect of treating the nanocrystals with different ligands was studied, observing that treatment with tetramethylammonium iodide generates films with intrinsic behavior. In the optimized device (6.3% certified efficiency), the $AgBiS_2$ layer was sandwiched between an electron transport/hole blocking substrate made from a thin layer of ZnO and an ultrathin electron blocking/hole transport PTB7 polymer layer. The promise of $AgBiS_2$ as a lead-free photovoltaic material is highlighted by a high short-circuit current of 22 mA/cm$^2$, with an active layer of only 35-nm thick. Furthermore, all the materials in the solar cell are non-toxic, and excluding the ITO layer and the metal contacts, all the layers are solution processed under ambient conditions and low temperatures.[88]

This study already identified some of the factor limiting performance: inefficient extraction of carriers at higher light intensities (especially for devices thicker than 50 nm), trap-assisted recombination processes, poor carrier transport, and incomplete extraction before recombination. Some possible solutions could be improvements in the synthesis, better nanocrystal passivation (ligand/surface treatments), introduction of light-trapping schemes, or nanostructuring of the active layer.

In another study, $AgBiS_2$ nanocrystals were obtained using an improved amine-based synthesis route.[89] Films fabricated with these nanocrystals showed improved carrier mobility, reduced carrier concentration, and improved photosensitivity, as compared to nanocrystals synthesized with oleic acid. This allowed us to fabricate solar cells with thicker active layers leading to improved efficiencies. Indeed, the optimal thickness of a champion solar cell was increased from 35 nm to 65 nm yielding a maximum efficiency of 4.3% using P3HT as a hole transport layer. This value compares well with previously reported values of 3.9% for a 35 nm thick device[88] and 2.6% for a 65 nm thick device fabricated with the oleic acid synthesis.

Recently, $AgBiS_2$ films were fabricated by spray pyrolysis.[90] In the optimized device, a 60–70 nm $AgBiS_2$ layer was integrated between a ZnO electron transport layer and a $MoO_3$-modified spiro-OMeTAD hole transport layer. Devices exhibited a maximum power-conversion efficiency of 1.5% with an aperture of 0.16 cm$^2$ and 1.2% for a larger area of 1 cm$^2$. Again, significant short-circuit currents were observed (18 mA/cm$^2$). When fabricating devices with active layers thicker than 70 nm, an enhancement in open-circuit voltage and field factor was observed but short-circuit current dramatically decreased. Interestingly, solar cells showed no degradation when stored for 1 month under diffuse light under ambient conditions at approximately 50% relative humidity and $24 \pm 2$ °C.

These studies point to the fact that with further work on $AgBiS_2$ efficiencies approaching those of the toxic counterparts could be achieved.

## VI. CONCLUSIONS AND FUTURE DIRECTIONS

In this Research perspective, we have summarized some of the bismuth-based materials that could serve as alternatives to the best performing, but highly toxic, materials used in perovskite or quantum dot solar cells. These materials fulfill the requirements of being composed of abundant and non-toxic elements. Moreover, they exhibit adequate properties for photovoltaics like high absorption coefficients and suitable bandgaps, plus additional attractive characteristics in terms of robustness and stability.

Apparently, one of the main limiting factors of these bismuth-based materials seems to be the anisotropy of the crystalline structures, forced by the presence of the ns$^2$ lone pair. This points to two routes to improve efficiency. On the one hand, take advantage of the anisotropic, low-dimensional crystalline structures by optimizing carrier transport through the growth of properly aligned and connected 1D structures (nanorods, nanowires, nanoribbons, etc.). On the other hand, identify more ternary compounds like $AgBiS_2$ which crystallize in symmetrical crystalline structures or perovskites that form higher dimensional octahedral networks. In this sense, a study explaining the difference in

crystalline structures for materials with alternate cations would be extremely interesting, especially if it could predict the crystalline structure of these compositions.

Even more, these materials have surprisingly received little attention. As a result, strategies that have proven successful in analogous systems—including alloying, doping, surface treatments with ligands, adequate alignment of semiconductors, or formation of bulk heterojunctions—remain largely unexplored.[91–94] These areas would be of interest in future studies and could further improve the efficiency of devices based on these abundant, non-toxic materials.

Finally, bismuth-based materials find applications in other optoelectronic devices like photodetectors,[95–97] photocatalytic processes like solar-driven hydrogen production or light degradation of pollutants,[98–100] other clean-energy devices like batteries or thermoelectric devices,[82,101–104] and as theragnostic agents (bioimaging + photothermal therapy).[105–107] All these areas will benefit from a better understanding and improvement of the properties of bismuth-based materials.

## ACKNOWLEDGMENTS

[1] See https://www.nrel.gov/pv/assets/images/efficiency-chart.png for efficiency-chart.png ($2219 \times 1229$) (2017); accessed 19 January 2018.

[2] C. Wadia, A. P. Alivisatos, and D. M. Kammen, "Materials availability expands the opportunity for large-scale photovoltaics deployment," Environ. Sci. Technol. **43**, 2072–2077 (2009).

[3] P. C. K. Vesborg and T. F. Jaramillo, "Addressing the terawatt challenge: Scalability in the supply of chemical elements for renewable energy," RSC Adv. **2**, 7933 (2012).

[4] M. Liu *et al.*, "Hybrid organic-inorganic inks flatten the energy landscape in colloidal quantum dot solids," Nat. Mater. **16**, 258–263 (2017).

[5] E. M. Sanehira *et al.*, "Enhanced mobility CsPbI$_3$ quantum dot arrays for record-efficiency, high-voltage photovoltaic cells," Sci. Adv. **3**, eaao4204 (2017).

[6] W. S. Yang *et al.*, "Iodide management in formamidinium-lead-halide–based perovskite layers for efficient solar cells," Science **356**, 1376–1379 (2017).

[7] WHO, *Ten Chemicals of Major Public Health Concern* (WHO, 2016).

[8] A. Babayigit, H.-G. Boyen, and B. Conings, "Environment versus sustainable energy: The case of lead halide perovskite-based solar cells," MRS Energy Sustainability **5**, E1 (2018).

[9] J. L. DiMeglio and J. Rosenthal, "Selective conversion of CO$_2$ to CO with high efficiency using an inexpensive bismuth-based electrocatalyst," J. Am. Chem. Soc. **135**, 8798–8801 (2013).

[10] R. Mohan, "Green bismuth," Nat. Chem. **2**, 336 (2010).

[11] A. M. Ganose, C. N. Savory, and D. O. Scanlon, "Beyond methylammonium lead iodide: Prospects for the emergent field of ns$^2$ containing solar absorbers," Chem. Commun. **53**, 20–44 (2017).

[12] R. E. Brandt, V. Stevanovi, D. S. Ginley, and T. Buonassisi, "Identifying defect-tolerant semiconductors with high minority-carrier lifetimes: Beyond hybrid lead halide perovskites," MRS Commun. **5**, 265–275 (2015).

[13] M. A. Green, Y. Jiang, A. M. Soufiani, and A. Ho-Baillie, "Optical properties of photovoltaic organic-inorganic lead halide perovskites," J. Phys. Chem. Lett. **6**, 4774–4785 (2015).

[14] S. D. Stranks *et al.*, "Electron-hole diffusion lengths exceeding 1 micrometer in an organometal trihalide perovskite absorber," Science **342**, 341–344 (2013).

[15] G. Han *et al.*, "Towards high efficiency thin film solar cells," Prog. Mater. Sci. **87**, 246–291 (2017).

[16] M. Lyu, J. H. Yun, P. Chen, M. Hao, and L. Wang, "Addressing toxicity of Lead: Progress and applications of low-toxic metal halide perovskites and their derivatives," Adv. Energy Mater. **7**, 1602512 (2017).

[17] M. Konstantakou and T. Stergiopoulos, "A critical review on tin halide perovskite solar cells," J. Mater. Chem. A **5**, 11518–11549 (2017).

[18] K. M. Boopathi *et al.*, "Solution-processable antimony-based light-absorbing materials beyond lead halide perovskites," J. Mater. Chem. A **5**, 20843–20850 (2017).

[19] C. Zhang, L. Gao, S. Hayase, and T. Ma, "Current advancements in material research and techniques focusing on lead-free perovskite solar cells," Chem. Lett. **46**, 1276–1284 (2017).

[20] O. Lindqvist, G. Johansson, F. Sandberg, and T. Norin, "The crystal structure of cesium bismuth iodide, Cs$_3$Bi$_2$I$_9$," Acta Chem. Scand. **22**, 2943–2952 (1968).

[21] B. W. Park *et al.*, "Bismuth based hybrid perovskites A$_3$Bi$_2$I$_9$ (A: Methylammonium or cesium) for solar cell application," Adv. Mater. **27**, 6806–6813 (2015).

[22] Z. Yang *et al.*, "Unraveling the exciton binding energy and the dielectric constant in single-crystal methylammonium lead triiodide perovskite," J. Phys. Chem. Lett. **8**, 1851–1855 (2017).

[23] A. Miyata *et al.*, "Direct measurement of the exciton binding energy and effective masses for charge carriers in organic-inorganic tri-halide perovskites," Nat. Phys. **11**, 582–587 (2015).

[24] H.-H. Fang *et al.*, "Photoexcitation dynamics in solution-processed formamidinium lead iodide perovskite thin films for solar cell applications," Light: Sci. Appl. **5**, e16056 (2015).

[25] B. Ghosh *et al.*, "Poor photovoltaic performance of $Cs_3Bi_2I_9$: An insight through first-principles calculations," J. Phys. Chem. C **121**, 17062–17067 (2017).

[26] T. Singh, A. Kulkarni, M. Ikegami, and T. Miyasaka, "Effect of electron transporting layer on bismuth-based lead-free perovskite $(CH_3NH_3)_3Bi_2I_9$ for photovoltaic applications," ACS Appl. Mater. Interfaces **8**, 14542–14547 (2016).

[27] M. Lyu *et al.*, "Organic–inorganic bismuth (III)-based material: A lead-free, air-stable and solution-processable light-absorber beyond organolead perovskites," Nano Res. **9**, 692–702 (2016).

[28] R. L. Z. Hoye *et al.*, "Methylammonium bismuth iodide as a lead-free, stable hybrid organic-inorganic solar absorber," Chem. - Eur. J. **22**, 2605–2610 (2016).

[29] Q. Li *et al.*, "High pressure band gap engineering in lead-free $Cs_2AgBiBr_6$ double perovskite," Angew. Chem., Int. Ed. **56**, 15969–15973 (2017).

[30] M. Vigneshwaran *et al.*, "Facile synthesis and characterization of sulfur doped low bandgap bismuth based perovskites by soluble precursor route," Chem. Mater. **28**, 6436–6440 (2016).

[31] K.-H. Hong, J. Kim, L. Debbichi, H. Kim, and S. H. Im, "Band gap engineering of $Cs_3Bi_2I_9$ perovskites with trivalent atoms using a dual metal cation," J. Phys. Chem. C **121**, 969–974 (2017).

[32] C. Ran *et al.*, "Construction of compact methylammonium bismuth iodide film promoting lead-free inverted planar heterojunction organohalide solar cells with open-circuit voltage over 0.8 V," J. Phys. Chem. Lett. **8**, 394–400 (2017).

[33] Z. Zhang *et al.*, "High-quality $(CH_3NH_3)_3Bi_2I_9$ film-based solar cells: Pushing efficiency up to 1.64%," J. Phys. Chem. Lett. **8**, 4300–4307 (2017).

[34] E. Greul, M. L. Petrus, A. Binek, P. Docampo, and T. Bein, "Highly stable, phase pure $Cs_2AgBiBr_6$ double perovskite thin films for optoelectronic applications," J. Mater. Chem. A **5**, 19972–19981 (2017).

[35] W. Gao *et al.*, "High quality $Cs_2AgBiBr_6$ double perovskite film for lead-free inverted planar heterojunction solar cells with 2.2% efficiency," ChemPhysChem (published online, 2018).

[36] Y. Kim *et al.*, "Pure cubic-phase hybrid iodobismuthates $AgBi_2I_7$ for thin-film photovoltaics," Angew. Chem., Int. Ed. **55**, 9586–9590 (2016).

[37] A. J. Lehner *et al.*, "Electronic structure and photovoltaic application of $BiI_3$," Appl. Phys. Lett. **107**, 131109 (2015).

[38] R. E. Brandt *et al.*, "Investigation of bismuth triiodide ($BiI_3$) for photovoltaic applications," J. Phys. Chem. Lett. **6**, 4297–4302 (2015).

[39] U. H. Hamdeh *et al.*, "Solution-processed $BiI_3$ thin films for photovoltaic applications: Improved carrier collection via solvent annealing," Chem. Mater. **28**, 6567–6574 (2016).

[40] X. Huang, S. Huang, P. Biswas, and R. Mishra, "Band gap insensitivity to large chemical pressures in ternary bismuth iodides for photovoltaic applications," J. Phys. Chem. C **120**, 28924–28932 (2016).

[41] T. Li *et al.*, "Lead-free pseudo-three-dimensional organic–inorganic iodobismuthates for photovoltaic applications," Sustainable Energy Fuels **1**, 308–316 (2017).

[42] A. J. Lehner *et al.*, "Crystal and electronic structures of complex bismuth iodides $A_3Bi_2I_9$(A = K, Rb, Cs) related to perovskite: Aiding the rational design of photovoltaics," Chem. Mater. **27**, 7137–7148 (2015).

[43] C. W. M. Timmermans, S. O. Cholakh, R. L. van der Woude, and G. Blasse, "Some optical and electrical measurements on $Cs_3Bi_2Br_9$ single crystals," Phys. Status Solidi B **115**, 267–271 (1983).

[44] M. I. Saidaminov, O. F. Mohammed, and O. M. Bakr, "Low-dimensional-networked metal halide perovskites: The next big thing," ACS Energy Lett. **2**, 889–896 (2017).

[45] I. C. Smith, E. T. Hoke, D. Solis-Ibarra, M. D. McGehee, and H. I. A. Karunadasa, "Layered hybrid perovskite solar-cell absorber with enhanced moisture stability," Angew. Chem., Int. Ed. **53**, 11232–11235 (2014).

[46] J. H. Lee, J. H. Lee, E. H. Kong, and H. M. Jang, "The nature of hydrogen-bonding interaction in the prototypic hybrid halide perovskite, tetragonal $CH_3NH_3PbI_3$," Sci. Rep. **6**, 1–12 (2016).

[47] S. Sun *et al.*, "Synthesis, crystal structure, and properties of a perovskite-related bismuth phase, $(NH_4)_3Bi_2I_9$," APL Mater. **4**, 031101 (2016).

[48] K. Eckhardt *et al.*, "Crystallographic insights into $(CH_3NH_3)_3(Bi_2I_9)$: A new lead-free hybrid organic–inorganic material as a potential absorber for photovoltaics," Chem. Commun. **52**, 3058–3060 (2016).

[49] E. T. McClure, M. R. Ball, W. Windl, and P. M. Woodward, "$Cs_2AgBiX_6$ (X = Br, Cl): New visible light absorbing, lead-free halide perovskite semiconductors," Chem. Mater. **28**, 1348–1354 (2016).

[50] G. Konstantatos, L. Levina, J. Tang, and E. H. Sargent, "Sensitive solution-processed $Bi_2S_3$ nanocrystalline photodetectors," Nano Lett. **8**, 4002–4006 (2008).

[51] L. Cademartiri *et al.*, "Large-scale synthesis of ultrathin $Bi_2S_3$ necklace nanowires," Angew. Chem., Int. Ed. **47**, 3814–3817 (2008).

[52] M. Bernechea, Y. Cao, and G. Konstantatos, "Size and bandgap tunability in $Bi_2S_3$ colloidal nanocrystals and its effect in solution processed solar cells," J. Mater. Chem. A **3**, 20642–20648 (2015).

[53] A. K. Rath, M. Bernechea, L. Martinez, and G. Konstantatos, "Solution-processed heterojunction solar cells based on p-type PbS quantum dots and n-type $Bi_2S_3$ nanocrystals," Adv. Mater. **23**, 3712–3717 (2011).

[54] L. Martinez, M. Bernechea, F. P. G. de Arquer, and G. Konstantatos, "Near IR-sensitive, non-toxic, polymer/nanocrystal solar cells employing $Bi_2S_3$ as the electron acceptor," Adv. Energy Mater. **1**, 1029–1035 (2011).

[55] A. K. Rath *et al.*, "Solution-processed inorganic bulk nano-heterojunctions and their application to solar cells," Nat. Photonics **6**, 529–534 (2012).

[56] L. Martinez *et al.*, "Hybrid solution-processed bulk heterojunction solar cells based on bismuth sulfide nanocrystals," Phys. Chem. Chem. Phys. **15**, 5482–5487 (2013).

[57] L. Martinez *et al.*, "Improved electronic coupling in hybrid organic–inorganic nanocomposites employing thiol-functionalized P3HT and bismuth sulfide," Nanoscale **6**, 10018 (2014).

[58] S. K. Saha and A. J. Pal, "Schottky diodes between $Bi_2S_3$ nanorods and metal nanoparticles in a polymer matrix as hybrid bulk-heterojunction solar cells," J. Appl. Phys. **118**, 014503 (2015).

[59] A. Walsh, D. J. Payne, R. G. Egdell, and G. W. Watson, "Stereochemistry of post-transition metal oxides: Revision of the classical lone pair model," Chem. Soc. Rev. **40**, 4455 (2011).

[60] L. A. Olsen, J. Lpez-Solano, A. Garca, T. Balić-Unić, and E. Makovicky, "Dependence of the lone pair of bismuth on coordination environment and pressure: An *ab initio* study on $Cu_4Bi_5S_{10}$ and $Bi_2S_3$," J. Solid State Chem. **183**, 2133–2143 (2010).

[61] H. Bao *et al.*, "Synthesis of a highly ordered single-crystalline $Bi_2S_3$ nanowire array and its metal/semiconductor/metal back-to-back Schottky diode," Small **4**, 1125–1129 (2008).

[62] Y. Cao *et al.*, "Solution processed bismuth sulfide nanowire array core/silver sulfide shell solar cells," Chem. Mater. **27**, 3700–3706 (2015).

[63] L. Whittaker-Brooks *et al.*, "$Bi_2S_3$ nanowire networks as electron acceptor layers in solution-processed hybrid solar cells," J. Mater. Chem. C **3**, 2686–2692 (2015).

[64] C. Coughlan *et al.*, "Compound copper chalcogenide nanocrystals," Chem. Rev. **117**, 5865–6109 (2017).

[65] H. Fu, "Environment-friendly and earth-abundant colloidal chalcogenide nanocrystals for photovoltaic applications," J. Mater. Chem. C **6**, 414–445 (2018).

[66] A. Zakutayev, "Brief review of emerging photovoltaic absorbers," Curr. Opin. Green Sustainable Chem. **4**, 8–15 (2017).

[67] S. G. Deshmukh and V. Kheraj, "A comprehensive review on synthesis and characterizations of $Cu_3BiS_3$ thin films for solar photovoltaics," Nanotechnol. Environ. Eng. **2**, 15 (2017).

[68] D. J. Temple, A. B. Kehoe, J. P. Allen, G. W. Watson, and D. O. Scanlon, "Geometry, electronic structure, and bonding in $CuMCh_2(M = Sb, Bi; Ch = S, Se)$: Alternative solar cell absorber materials?," J. Phys. Chem. C **116**, 7334–7340 (2012).

[69] J. T. R. Dufton *et al.*, "Structural and electronic properties of $CuSbS_2$ and $CuBiS_2$: Potential absorber materials for thin-film solar cells," Phys. Chem. Chem. Phys. **14**, 7229 (2012).

[70] M. Kumar and C. Persson, "$CuSbS_2$ and $CuBiS_2$ as potential absorber materials for thin-film solar cells," J. Renewable Sustainable Energy **5**, 031616 (2013).

[71] N. Suriyawong, B. Aragaw, J. B. Shi, and M. W. Lee, "Ternary $CuBiS_2$ nanoparticles as a sensitizer for quantum dot solar cells," J. Colloid Interface Sci. **473**, 60–65 (2016).

[72] J.-J. Wang, M. Z. Akgul, Y. Bi, S. Christodoulou, and G. Konstantatos, "Low-temperature colloidal synthesis of $CuBiS_2$ nanocrystals for optoelectronic devices," J. Mater. Chem. A **5**, 24621–24625 (2017).

[73] M. Kumar and C. Persson, "$Cu(Sb,Bi)(S,Se)_2$ as indium-free absorber material with high optical efficiency," Energy Procedia **44**, 176–183 (2014).

[74] N. J. Gerein and J. A. Haber, "One-step synthesis and optical and electrical properties of thin film $Cu_3BiS_3$ for use as a solar absorber in photovoltaic devices," Chem. Mater. **18**, 6297–6302 (2006).

[75] M. Kumar and C. Persson, "$Cu_3BiS_3$ as a potential photovoltaic absorber with high optical efficiency," Appl. Phys. Lett. **102**, 062109 (2013).

[76] C. Yan *et al.*, "Colloidal synthesis and characterizations of wittichenite copper bismuth sulphide nanocrystals," Nanoscale **5**, 1789 (2013).

[77] J. Yin and J. Jia, "Synthesis of $Cu_3BiS_3$ nanosheet films on $TiO_2$ nanorod arrays by a solvothermal route and their photoelectrochemical characteristics," CrystEngComm **16**, 2795 (2014).

[78] J. Li *et al.*, "One–step synthesis of $Cu_3BiS_3$ thin films by a dimethyl sulfoxide (DMSO)–based solution coating process for solar cell application," Sol. Energy Mater. Sol. Cells **174**, 593–598 (2018).

[79] X. Liu, H. Zheng, J. Zhang, Y. Xiao, and Z. Wang, "Photoelectric properties and charge dynamics for a set of solid state solar cells with $Cu_4Bi_4S_9$ as the absorber layer," J. Mater. Chem. A **1**, 10703 (2013).

[80] X. Liu, S. Wang, J. Zhang, J. Zhang, and Y. Gu, "Photoelectric properties and charge dynamics in ZnO nanowires/$Cu_4Bi_4S_9$ and ZnO nanowires/$In_2O_3$/$Cu_4Bi_4S_9$ heterostructures," J. Appl. Phys. **116**, 245101 (2014).

[81] S. Wang, X. Y. Liu, and Y. Z. Gu, "Excellent photoelectric properties and charge dynamics of two types of bulk heterojunction solar cells," Mater. Lett. **166**, 251–254 (2016).

[82] S. N. Guin and K. Biswas, "Cation disorder and bond anharmonicity optimize the thermoelectric properties in kinetically stabilized rocksalt $AgBiS_2$ nanocrystals," Chem. Mater. **25**, 3225–3231 (2013).

[83] B. Pejova, D. Nesheva, Z. Aneva, and A. Petrova, "Photoconductivity and relaxation dynamics in sonochemically synthesized assemblies of $AgBiS_2$ quantum dots," J. Phys. Chem. C **115**, 37–46 (2011).

[84] B. Pejova, I. Grozdanov, D. Nesheva, and A. Petrova, "Size-dependent properties of sonochemically synthesized three-dimensional arrays of close-packed semiconducting $AgBiS_2$ quantum dots," Chem. Mater. **20**, 2551–2565 (2008).

[85] P. C. Huang, W. C. Yang, and M. W. Lee, "$AgBiS_2$ semiconductor-sensitized solar cells," J. Phys. Chem. C **117**, 18308–18314 (2013).

[86] S. Zhou *et al.*, "Preparation and photovoltaic properties of ternary $AgBiS_2$ quantum dots sensitized $TiO_2$ nanorods photoanodes by electrochemical atomic layer deposition," J. Electrochem. Soc. **163**, D63–D67 (2016).

[87] N. Liang *et al.*, "Homogenously hexagonal prismatic $AgBiS_2$ nanocrystals: controlled synthesis and application in quantum dot-sensitized solar cells," CrystEngComm **17**, 1902–1905 (2015).

[88] M. Bernechea *et al.*, "Solution-processed solar cells based on environmentally friendly $AgBiS_2$ nanocrystals," Nat. Photonics **10**, 521–525 (2016).

[89] L. Hu *et al.*, "Enhanced optoelectronic performance in $AgBiS_2$ nanocrystals from an improved amine-based synthesis route," J. Mater. Chem. C **6**, 731–737 (2018).

[90] N. Pai *et al.*, "Spray deposition of $AgBiS_2$ and $Cu_3BiS_3$ thin films for photovoltaic applications," J. Mater. Chem. C **6**, 2483–2494 (2018).

[91] G. H. Carey *et al.*, "Colloidal quantum dot solar cells," Chem. Rev. **115**, 12732–12763 (2015).

[92] F. Liu *et al.*, "Colloidal synthesis of air-stable alloyed $CsSn_{1-x}Pb_xI_3$ perovskite nanocrystals for use in solar cells," J. Am. Chem. Soc. **139**, 16708 (2017).

[93] M. Yuan, M. Liu, and E. H. Sargent, "Colloidal quantum dot solids for solution-processed solar cells," Nat. Energy **1**, 16016 (2016).

[94] C. R. Kagan and C. B. Murray, "Charge transport in strongly coupled quantum dot solids," Nat. Nanotechnol. **10**, 1013–1026 (2015).

[95] J. Chao *et al.*, "Large-scale synthesis of $Bi_2S_3$ nanorods and nanoflowers for flexible near-infrared laser detectors and visible light photodetectors," Mater. Res. Bull. **98**, 194–199 (2018).

[96] W. Huang *et al.*, "Facile fabrication and characterization of two-dimensional bismuth(III) sulfide nanosheets for high-performance photodetector applications under ambient conditions," Nanoscale **10**, 2404–2412 (2018).

[97] H. Yu *et al.*, "Scalable colloidal synthesis of uniform $Bi_2S_3$ nanorods as sensitive materials for visible-light photodetectors," CrystEngComm **19**, 727–733 (2017).

[98] A. Sarkar *et al.*, "Enhanced photocatalytic performance of morphologically tuned $Bi_2S_3$ NPs in the degradation of organic pollutants under visible light irradiation," J. Colloid Interface Sci. **483**, 49–59 (2016).

[99] X. Meng and Z. Zhang, "Bismuth-based photocatalytic semiconductors: Introduction, challenges and possible approaches," J. Mol. Catal. A: Chem. **423**, 533–549 (2016).

[100] H. Abdullah and D.-H. Kuo, "Photocatalytic performance of Ag and $CuBiS_2$ nanoparticle-coated $SiO_2$@$TiO_2$ composite sphere under visible and ultraviolet light irradiation for azo dye degradation with the assistance of numerous nano p–n diodes," J. Phys. Chem. C **119**, 13632–13641 (2015).

[101] J. Ni *et al.*, "Strongly coupled $Bi_2S_3$@CNT hybrids for robust lithium storage," Adv. Energy Mater. **4**, 1400798 (2014).

[102] G. Nie, X. Lu, J. Lei, L. Yang, and C. Wang, "Facile and controlled synthesis of bismuth sulfide nanorods-reduced graphene oxide composites with enhanced supercapacitor performance," Electrochim. Acta **154**, 24–30 (2015).

[103] W. Yang, H. Wang, T. Liu, and L. Gao, "A $Bi_2S_3$@CNT nanocomposite as anode material for sodium ion batteries," Mater. Lett. **167**, 102–105 (2016).

[104] K. Biswas, L. D. Zhao, and M. G. Kanatzidis, "Tellurium-free thermoelectric: The anisotropic n-type semiconductor $Bi_2S_3$," Adv. Energy Mater. **2**, 634–638 (2012).

[105] Y. Cheng *et al.*, "Deep-level defect enhanced photothermal performance of bismuth sulfide–gold heterojunction nanorods for photothermal therapy of cancer guided by computed tomography imaging," Angew. Chem., Int. Ed. **57**, 246–251 (2018).

[106] Y. Yang *et al.*, "Hydrophilic $Cu_3BiS_3$ nanoparticles for computed tomography imaging and photothermal therapy," Part. Part. Syst. Charact. **32**, 668–679 (2015).

[107] Z. Li *et al.*, "Untrasmall $Bi_2S_3$ nanodots for *in vivo* X-ray CT imaging-guided photothermal therapy of cancer," RSC Adv. **7**, 29672–29678 (2017).